ADVANCING EARTH AND SPACE SCIENCE

JGR Atmospheres

RESEARCH ARTICLE
10.1029/2020JD033703

Key Points:

- The occurrences of long-lasting concentric eyewalls are documented in the western North Pacific, eastern Pacific, and Atlantic basins
- The environmental conditions critical for the maintenance of concentric eyewalls are examined, in addition to the internal dynamics
- Most of the triple eyewalls evolves to a concentric eyewall, and belongs to the long-lived category

Supporting Information:

Supporting Information may be found in the online version of this article.

Correspondence to:

B.-F. Chen,
bfchen@ntu.edu.tw

Citation:

Yang, Y.-T., Kuo, H.-C., Tsujino, S., Chen, B.-F., & Peng, M. S. (2021). Characteristics of the long-lived concentric eyewalls in tropical cyclones. *Journal of Geophysical Research: Atmospheres*, *126*, e2020JD033703. https://doi.org/10.1029/2020JD033703

Received 21 AUG 2020
Accepted 22 MAY 2021

Author Contributions:

Conceptualization: Hung-Chi Kuo, Satoki Tsujino, Buo-Fu Chen, Melinda S Peng
Formal analysis: Yi-Ting Yang, Satoki Tsujino, Buo-Fu Chen
Funding acquisition: Hung-Chi Kuo
Investigation: Yi-Ting Yang, Melinda S Peng
Methodology: Yi-Ting Yang, Hung-Chi Kuo, Satoki Tsujino, Buo-Fu Chen
Project Administration: Hung-Chi Kuo
Software: Yi-Ting Yang
Supervision: Hung-Chi Kuo
Validation: Yi-Ting Yang, Buo-Fu Chen
Writing – original draft: Yi-Ting Yang, Hung-Chi Kuo, Buo-Fu Chen
Writing – review & editing: Hung-Chi Kuo, Satoki Tsujino, Buo-Fu Chen, Melinda S Peng

Characteristics of the Long-Lived Concentric Eyewalls in Tropical Cyclones

Yi-Ting Yang[1], Hung-Chi Kuo[2], Satoki Tsujino[2], Buo-Fu Chen[3], and Melinda S Peng[4]

[1]Technology Education Division, National Science and Technology Museum, Kaohsiung, Taiwan, [2]Department of Atmospheric Sciences, National Taiwan University, Taipei, Taiwan, [3]Center for Weather Climate and Disaster Research, National Taiwan University, Taipei, Taiwan, [4]University of Colorado – Colorado Spring, Boulder, CO, USA

Abstract Concentric eyewalls (CEs) in tropical cyclones (TCs) in different basins were identified based on satellite imagery during 1997–2014. Their duration and structural parameters, including inner eyewall size, moat width, and outer eyewall width, were calculated. Differences in these parameters can best be distinguished by short-lived and long-lived CEs (i.e., CEs with durations shorter or longer than 20 h). A long-lived CE tends to have a larger size, mainly contributed by a larger moat and a larger outer eyewall width. The inner eyewall size shows no significant difference between short-lived and long-lived CEs in the western North Pacific (WNP) but increases slightly and steadily with increasing CE durations in the Atlantic (ATL). Furthermore, the WNP has far more CEs than in ATL and in the eastern Pacific (EPAC) for all duration categories. Long-lived CEs cover about 20% of all CEs and are associated with higher sea surface temperature and weaker vertical wind shear. In the WNP, the TC tracks associated with long-lived CEs were with the less northward motion component. Furthermore, seven TCs with triple eyewalls in the WNP are identified during 1997–2014, with only one case in the EPAC and no ATL case. It is found that five cases of these triple eyewalls TC in the WNP evolved to long-lived CEs. The results suggest that the CE internal dynamical process, the TC track during the CE period, and the environmental conditions are all critical to the CE size and duration.

1. Introduction

One of the challenges for tropical cyclone (TC) forecasting is to predict its potentially largely variable structure and intensity. Regarding this topic, the occurrence of a concentric eyewall (CE) is critical. A CE is identified by two axisymmetric wind maxima in the radial direction and the associated concentric convective rings (Black & Willoughby, 1992; Willoughby et al., 1982). In an eyewall replacement cycle (ERC), the outer eyewall develops and contracts as the inner eyewall collapses due to the outer eyewall blocking moisture and momentum transport. The TC generally weakens in maximum wind speed during this stage. Subsequently, the outer eyewall can replace the inner eyewall and the TC re-intensifies in maximum wind speed. Sitkowski et al. (2011) documented that the mean locations of the inner and outer wind maximum at the start of an ERC are 35 and 106 km from the storm center for Atlantic TCs. Furthermore, pioneer studies on the CE and ERC (Black & Willoughby, 1992; Willoughby et al., 1982) using aircraft observations also showed that a CE frequently occurs in an intense TC and plays an essential role in TC intensity change. Kuo et al. (2009) identified that 72% of Category 5% and 57% of Category 4 storms had CEs in the western North Pacific (WNP) based on microwave satellite data.

Using aircraft reconnaissance flight level data, Maclay et al. (2008) showed that while the intensity weakens during the ERC, the integrated kinetic energy and the TC size increase. They also suggested that internal dynamical processes dominate secondary eyewall formation and ERC. Sitkowski et al. (2011) indicated that the ERC might lead to increases in both storm size and integrated kinetic energy. During an ERC, the inner-core structure undergoes dramatic changes that result in an intensity oscillation and rapid broadening of the wind field.

In addition to a typical CE accompanied by an ERC, Yang et al. (2013) identified two other CE types in the WNP. Yang et al. (2013) used microwave satellite images from Naval Research Laboratory (NRL) between 1997 and 2010 and an objective method to identify (a) CE with an eyewall replacement cycle (ERC; 53%); (b) CE with no replacement cycle (NRC; 24%); and (c) CE that is maintained for an extended period longer than

20 h (i.e., long-lived CE; 23%). A long-lived CE maintains its convective rings for more than 20 h (with a 31-h mean). They suggested that the maintenance of the CE structure with the larger moat and outer eyewall width might be due to the storm-scale vorticity stabilization with barotropic instability (Kossin et al., 2000). The duration may be related to the large size of the CE.

It is considered that another unique species of CE is the triple eyewall. McNoldy (2004) first documented TCs with triple eyewalls. Zhao et al. (2016) investigated the triple eyewalls in Typhoon Usagi (2013). Tsujino et al. (2017) reported Typhoon Bolaven with triple eyewall from radar data. It is worth noting that the triple eyewall of Typhoon Bolaven has a prolonged duration (>20 h), according to the microwave satellite data. Although the physical mechanism contributing to triple eyewall formation is still unclear, the current study is motivated to investigate the climatological of triple eyewalls to get some hints to understand CEs with various durations.

Generally, CE duration covers the period from the formation of the secondary eyewall to its contraction and finally the replacement of the original decaying inner eyewall. However, the CE duration varies significantly according to previous studies. Aircraft observation of Hurricane Andrew in 1992 (Willoughby & Black, 1996) and radar observations of Typhoon Lekima in 2001 (Kuo et al., 2004; Yang et al., 2016) both indicated that the CE duration is approximately six hours. Sitkowski et al. (2011) used aircraft data and microwave satellite data to analyzed 24 ERC events and found that the average CE duration identified by aircraft data lasts for about 36 h, which is much longer than the 17.5-h duration estimated based on satellite data. The shorter CE duration identified based on satellite images is attributed to that the microwave sensor has to observe snow and ice particles associated with the concentric deep convective ring, which is generally present after the establishment of the secondary wind maxima (Sitkowski et al., 2011). The shorter CE duration may also be due to the fact that the aircraft data are one-direction profiles while satellite data are plane-view snapshots. On the other hand, the CE durations in numerical simulations such as Abarca and Corbosiero (2011), Ortt and Chen (2008), Terwey and Montgomery (2008), Zhou and Wang (2009), Qiu et al. (2010), Rozoff et al. (2012) and Montgomery et al. (2014) are in the range of 6–18 h, considerably shorter than the CE durations of real TCs (Sitkowski et al. 2011). A recent modeling study of Tsujino et al. (2017) suggested that the incomplete blocking of the outer eyewall to the inner eyewall moisture supply may prolong the CE duration.

As the TC generally re-intensifies after the ERC is complete, it is critical to understand the processes and factors affecting the CE duration to predict the TC intensity evolution. Yang et al. (2015) suggested that the CE duration in the WNP appears to be longer in an El Nino year. Besides, TCs with multiple CE formation in the El Nino years tend to have enlarged CE size. As the El Nino-Southern Oscillation (ENSO) substantially modified the synoptic environment for TC development in the WNP, it is implied that environmental conditions might also affect the CE size and CE duration to the internal dynamical processes (e.g., Kossin et al., 2000).

A further examination of how the environmental factors affect CE, particularly how they contribute to a prolonged CE duration, is motivated in this study. This study examines the relationship of CE duration with its structure and the environmental factors in different basins from 1997 to 2014, aiming to understand the characteristics of long-lived CEs (and triple eyewalls). By implementing an objective method similar to that of Yang et al. (2013), we use satellite microwave image, radar image, and cloud liquid water (CLW) to identify CEs and triple eyewalls, and then examine the characteristics of CE duration in different basins and associated environmental conditions. Section 2 describes the data and methodologies to characterize CEs. The results are presented in Section 3. Summary and discussion are provided in Section 4.

2. Data and Methodology

The low earth orbit (LEO) satellite passive microwave (PMW) sensors observe radiances from the Earth's surface, cloud emissions, and ice particles scatter. The PMW sensors are useful for TC internal structure monitoring, especially the 85–91 GHz channels (Hawkins et al., 2008; Willoughby, 1995). The colder brightness temperature (T_B) is caused by ice scattering associated with intense convection. As a result, the 85–91 GHz channels can provide inner eyewall, moat, and outer eyewall structures of CEs. Due to the PMW sensors with modest swath (1,300–1,700 km) onboard on LEO satellites, every satellite observes the same TC

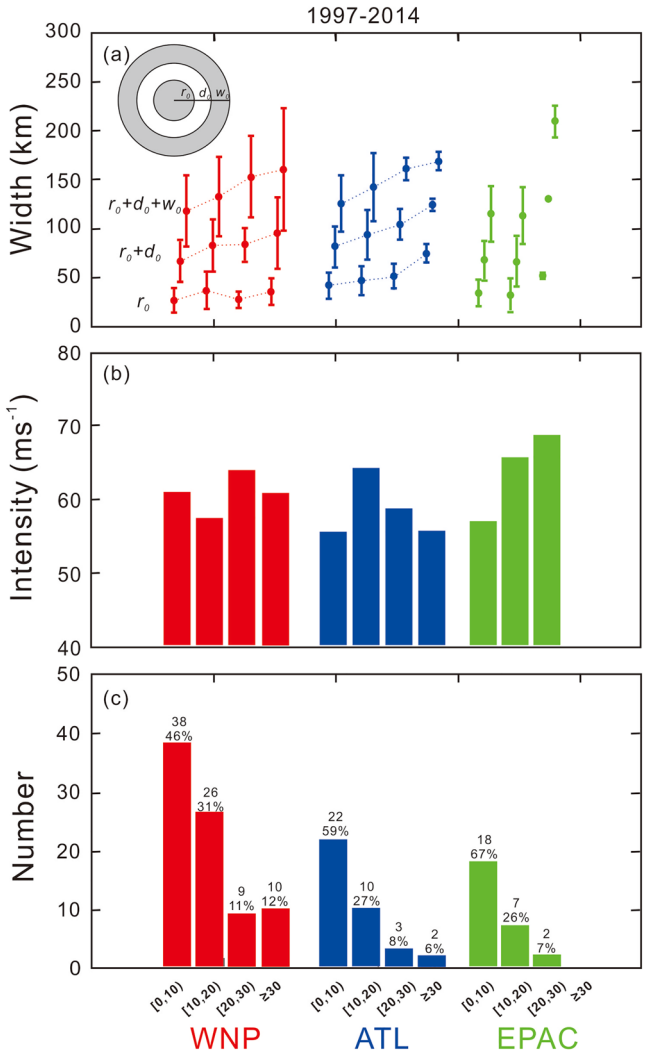

Figure 1. (a) The mean and standard deviation of r0, r0+d0, and r0+d0+w0 for concentric eyewall (CE) cases with 0–10 h, 10–20 h, 20–30 h, and longer than 30 h duration. The dashed lines connecting the mean sizes at different duration illustrate the trend. The green dash line is not plotted because there is no CE case with longer than 30 h duration. Note that the left bracket indicates equal or greater than the first number, and the right parenthesis indicates less than the second number enclosed. (b) (c) The mean intensity (b) the number with the percentage in each basin (c) for CE cases with 0–10 h, 10–20 h, 20–30 h, and longer than 30 h duration. The red, blue, and green represent the western North Pacific (WNP), Atlantic (ATL), and eastern Pacific (EPAC), respectively.

at most twice per day. By combining different PMW sensors, there would be in general a PMW sensor observation of a TC in every 3–6 h during a TC lifecycle. These PMW sensors including the passive Special Sensor Microwave Imager (SSM/I), the passive Tropical Rainfall Measuring Mission (TRMM) Microwave Imager (TMI), the Special Sensor Microwave Imager/Sounder (SSM/IS), the Global Precipitation Measurement (GPM) Microwave Imager (GMI), the Advanced Microwave Scanning Radiometer 2 (AMSR-2) data (Yang et al., 2014a, 2014b; Yang & Cossuth, 2016; Yang et al., 2020).

In this study, PMW images are used to identify and examine the characteristics and durations of CEs from 1997 to 2014 in the WNP, Atlantic (ATL), and eastern Pacific (EPAC) basins. In particular, we use the SSM/I 85-GHz observation and the passive Tropical Rainfall Measuring Mission (TRMM) Microwave Imager (TMI) data (Kummerow et al., 1998). These satellite images were obtained from the NRL Marine Meteorology Division in Monterey, California (Hawkins et al., 2001, 2006) and downloaded from the NRL TC webpage (https://www.nrlmry.navy.mil/TC.html). The NRL satellite microwave images are based on raw data reprocessed using the antenna gain function associated with the sampled radiometer data to create high-resolution (1–2 km) products that can be used in defining inner-storm structural details (Hawkins & Helveston, 2004, 2008). In addition to SSM/I and TMI data, the AMSR-E data are available starting from 2003, the SSM/IS data from 2005, the GMI data from 2014,the AMSR-2 data are from 2012. The data length is shorter than that of the SSM/I and TMI data. This study currently concentrates on the SSM/I and TMI data to give a comprehensive study for the CE climatology in a consistent manner.

We adopted the objective method in Yang et al. (2013) to identify CEs. The domain centered at the storm is divided into eight azimuthal sections with 45° each. The radial profile of the brightness temperature (T_B) across the center is examined, and criteria selected in Yang et al. (2013) are used to determine whether a storm has a CE and its inner core size, moat width, and outer eyewall width are estimated. Specifically, eight radial profiles of T_B are used to identify the CE cases, following five sequential steps:

(1) Find the possible moat location: check for the existence of one local maximum T_B (weak convection) between two minimum T_B (strong convection) in each profile
(2) Check the significance of the moat: check in each profile that the local T_B maximum and minimum satisfy the criteria of $T_{B\_max} \geqq \sigma_{outer\_min} + T_{B\_outer\_min}$ and $T_{B\_max} \geqq \sigma_{inner\_min} + T_{B\_inner\_min}$
(3) Check the existence of strong outer convection: check if $T_{B\_outer\_min} \leqq$ 230K in each profile that satisfies the criteria (1) and (2)
(4) Check symmetric structure: Check if at least 5 out of 8 sectors/profiles satisfy the above three criteria
(5) Check the outer convection is not a spiral rainband: Check if the radial distance between any sectors of the two outer eyewalls is smaller than 50 km

Where the $T_{B\_inner\_min}$, T_{B_max}, and $T_{B\_outer\_min}$ represent the minimum T_B near the inner core, local maximum T_B between inner and outer T_B, and the minimum T_B near the outer eyewall from the inner core. The σ_{inner_min} (σ_{outer_min}) represents the standard deviation of the minimum T_B near the inner core (near outer eyewall) calculated by each radial profile. Inserted in the upper left corner in Figure 1 is the schematic illustration of structure parameters for a CE, represented by the radial distance r_0, d_0, and w_0. The r_0 is the radius of the

outer edge of the inner eyewall; it is defined as the distance between the typhoon center to the point where $T_B = 0.5 \times \sigma_{inner} + T_{B\_inner}$. The w_0 is the outer eyewall width, which is defined as the radial distance of the region that satisfies $T_B < 0.5 \times \sigma_{outer} + T_{B\_outer}$ in the outer eyewall region. The d_0, moat width, covers the radii of $T_B \geq 0.5 \times \sigma_{outer} + T_{B\_outer}$ and $T_B \geq 0.5 \times \sigma_{inner} + T_{B\_inner}$. A more detailed discussion of this methodology can be found in Section 2 of Yang et al. (2013).

After identifying the CE presence in every PMW image, the CE duration is defined as from the first CE image to the last CE image. To avoid identifying the multiple CE cases into a long-lived CE structure due to the inadequate temporal resolution in the microwave data, a CE must maintain a similar inner core size. Finally, we further removed CE cases that made landfall during the CE period; thus, this left 83, 34, and 26 CE cases between 1997 and 2014 in the WNP, ATL, and EPAC basins, respectively (Please see the supplemental tables).

While the secondary eyewalls are subject of interest in the TC research, TC with triple eyewalls is known to exist (McNoldy, 2004; Tsujino et al., 2017; Zhao et al., 2016). We extend the objective method of Yang et al. (2013) to the identification of triple eyewalls. The identification of the secondary moat is similar to that of the inner moat. The tertiary outer eyewall is identified with T_B less than 240 K rather than 230 K as in Yang et al. (2013). The algorithm may be sensitive to the convection of the tertiary eyewall. The 240-K threshold seems to identify TCs with triple eyewalls, which agrees with previous observations such as McNoldy (2004). Furthermore, we confirm that this outer convection is not a spiral rainband if the difference in the outer eyewall radius between any of the eight sectors is smaller than 50 km.

To examine the environmental conditions associated with CEs, the Statistical Hurricane Intensity Prediction Scheme (SHIPS) and Statistical Typhoon Intensity Prediction Scheme (STIPS) are used. SHIPS system combines climatological, persistence, and synoptic predictors to forecast intensity changes using a multiple regression technique. The original version of SHIPS was developed in 1993 (DeMaria & Kaplan, 1994). In 1996, the system was incorporated into the National Hurricane Center operational forecast application. The development of STIPS closely follows the development of the SHIPS model in the ATL and EPAC basins (DeMaria & Kaplan, 1999; DeMaria et al., 2005; Knaff et al., 2005).

The column-integrated CLW path data are used to estimate the moisture content in the TC inner-core of CEs. The CLW data are produced by Remote Sensing Systems and are available at www.remss.com/missions/ssmi. Because the low-frequency microwave channels fully penetrate virtually all clouds, they can directly measure the total liquid cloud condensate amount (Greenwald et al., 1995; Lin & Rossow, 1994; Liu & Curry, 1993; Petty, 1990). The CLW data used in this study are based on SSM/I microwave retrieval products calculated at Remote Sensing Systems (RSS) and gridded daily data for both descending and ascending overpasses at the 0.25° resolution (http://www.remss.com). The CLW data used here is from Version 7 (Wentz & Meissner, 2000; Wentz, 2013). For valid pixels, the retrieval algorithm uses 19, 22, and 37 GHz frequency channels. To analyze the relationship between the CE duration and CE size, the domain size for the computation of CLW is $\left\{2 \times \left[\left(r_0 + d_0 + w_0\right) + 25\right]\right\}$ km $\times \left\{2 \times \left[\left(r_0 + d_0 + w_0\right) + 25\right]\right\}$ km for each CE cases, where r_0, d_0, and w_0 are obtained from the objective method. Cases with no available data on more than 20% of this grid are excluded, and interpolation between time slots is used instead.

3. Results: Characteristics of Concentric Eyewalls

3.1. Structural Characteristics of Long-Lived and Short-Lived CEs

We analyzed the CE duration and structural characteristics of 83, 34, and 26 CE cases during 1997–2014 in the WNP, ATL, and EPAC basins, respectively (Figure 1). There are 10 cases (11%) in which the CE structure is maintained longer than 30 h in the WNP while there are only two such cases (6%) in the ATL. These extremely long-lived CE cases are, on average, with larger moat and wider outer eyewall as compared with that of the TC with CE duration time less than 20 h (Figure 1a). In particular, the long-lived cases have larger moats (58-km mean in WNP, 36-km mean in ATL) and larger outer eyewall widths (67-km mean in WNP, 36-km mean in ATL). These characteristics are detected in both basins and more evident in the WNP

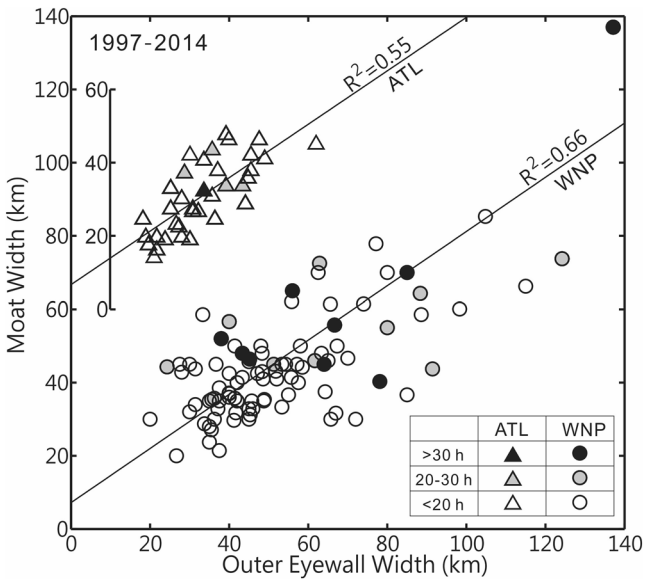

Figure 2. Scatter diagram of the moat width versus outer eyewall width. The moat widths for concentric eyewall (CE) cases in the Atlantic (ATL) basin are lifted 60 km for clarity (the smaller scales inside the diagram indicate actual values). The triangles and circles represent cases in the ATL and western North Pacific (WNP) basins, respectively. The white, gray, and black indicate various CE durations (see the inset). The linear fitting line and R2 are also shown.

basin than in the ATL basin. The average CE duration for all WNP and ATL cases is 16 and 10 h, with large standard deviations of 13 and 8 h, respectively.

Also shown in Figure 1a, the dashed lines reveal the trends of the CE size parameters. The trend for EPAC cases was not plotted because of its smaller sample number. The mean inner eyewall size for WNP cases is smaller than that for ATL cases, and they are not distinctive with different CE durations. Meanwhile, the inner eyewall size for ATL cases increases appreciably with the increasing duration. The moat size and the outer eyewall size increase with the duration time for WNP cases, and their corresponding increase is less for ATL cases. Finally, the overall size measured by $r_0 + d_0 + w_0$ is comparable in the WNP and ATL, and both increase with duration. The overall size increases primarily come from the inner eyewall size increase in ATL and from both the moat size and the outer eyewall size increases in WNP.

The averaged TC intensity at the CE formation time for each group with a different duration is given in Figure 1b. There is no apparent correlation between TC intensity and CE duration in the WNP or ATL basins. For EPAC cases, the TC intensity increases as the CE duration increases, but we would not emphasize its significance due to the smaller sample number in the EPAC. Generally, the CE duration bears little correlation with the TC intensity at the CE formation time. Note that some uncertainty of this relationship may be attributed to the usage of best-track intensities based primarily on Dvorak technique, which often fails to capture intensity fluctuations during an ERC.

The numbers of cases with different CE durations are provided (Figure 1c). The WNP has the largest numbers in all categories, followed by ATL and then the EPAC. The ATL and EPAC have a higher percentage of CEs with a duration <10 h. In the group of [10,20), the percentage is close in the three basins with around 30% values. Both the actual number and percentage drop significantly moving in the long-lived categories (≥20 h).

To further explore the structural characteristics of CE, the scatter plot of the moat width and outer eyewall width are displayed in Figure 2. Long-lived cases in various basins have moat widths greater than 35 (32) km in the WNP (ATL). The distribution indicates that the outer eyewall width is larger with a larger moat width ($R^2 = 0.66$ in WNP and 0.55 in ATL, where R^2 is the squared correlation coefficient measuring how close the data are to the fitted regression line). This is consistent with the trend shown in Figure 1a, and the trend of the moat and outer eyewall width are pronounced in the WNP. Kossin et al. (2000) identified two types of barotropic instabilities in the vorticity field with CE structure; the instabilities across the outer eyewall (type I) and the moat (type II) due to the sign reversal of the radial vorticity gradient (i.e., the Rayleigh necessary condition). These instabilities may work against the maintenance of the CE structure. The large moat size in the long-lived cases has two dynamic implications. It reduces the growth rate of the type II instability across the moat, which is favorable for the CE structure maintenance; and it also lessens the stabilization of the core vortex on the type I instability across the outer eyewall (i.e., the Fjørtoft sufficient condition), which is not favorable for the CE maintenance. As Kossin et al. (2000) demonstrated, the thicker outer eyewall is more stable for the type I instability, which is favorable for maintaining the outer eyewall structure. These observations of the large outer eyewall and moat widths are in general agreement with the concept that barotropic dynamics may play a significant role in maintaining the CE structure for long-lived CEs.

We use the CLW as the proxy for the TC inner-core convective activities and examine its correlation with the size distribution and eyewall profile. Scatter plots between CLW (area coverage of it given in Section 1) and outer eyewall area ($\sim w_0^2$), and between CLW and total size ($r_0 + d_0 + w_0$) are shown in Figure 3. The correlations between CLW and outer eyewall area are $R^2 = 0.89$ in WNP and $R^2 = 0.7$in ATL; both are positively correlated. Furthermore, the correlations between CLW and size are $R^2 = 0.72$ in the WNP basin and

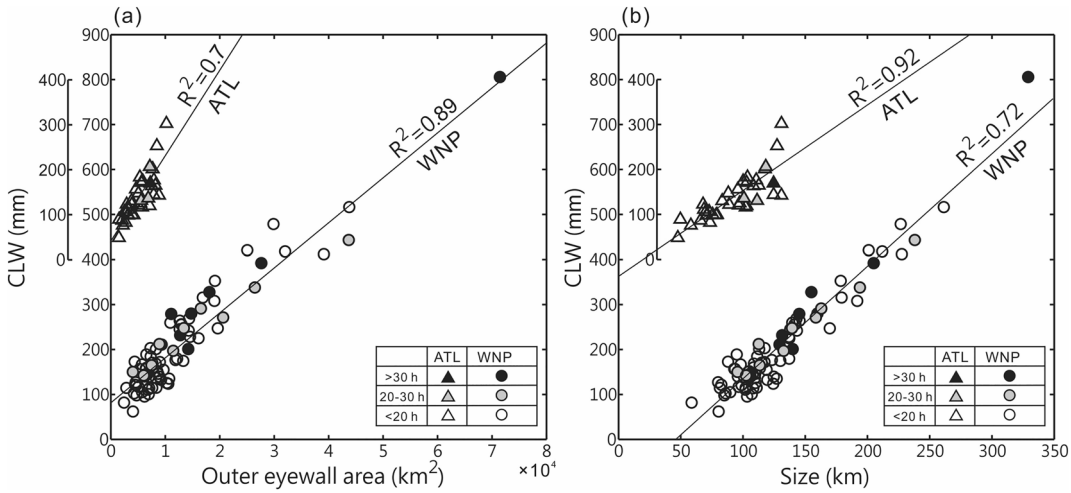

Figure 3. Scatter diagram of the cloud liquid water (CLW) versus (a) outer eyewall area and (b) CE size (r0+d0+w0). The CLW of concentric eyewall (CE) cases in the ATL basin is lifted 400 g m-2 upward for clarity. The triangles and circles represent cases in the Atlantic (ATL) and western North Pacific (WNP) basin, respectively. The white, gray, and black indicate CE various durations (see the inset). The linear fitting line and R2 are also shown.

$R^2 = 0.92$ in ATL. The correlations between CLW and outer eyewall area and between CLW and total size are high in both basins.

In summary, the outer eyewall width is larger with a larger moat width. On the other hand, the inner eyewall radius, in general, is smaller than the moat width and outer eyewall width. As a result, the large moat and large outer eyewall result in an overall large TC size. Also, the CLW of CE has a good correlation with the outer eyewall area and overall size. Recalling in Figure 1a that the WNP cases have larger moat size and the outer eyewall size, it is possible that the large moat size and wider outer eyewall maybe with a better barotropic vorticity stabilization to maintain the CE vorticity structure and delay the ERC (Kossin et al., 2000; Kuo et al., 2009). Thus, WNP cases have a higher probability of becoming a long-lived CE (Figure 1c).

3.2. Multiple CE Formation, Triple Eyewalls, and Maintained Durations

As the large size of the moat and outer eyewall width are essential characters of long-lived cases, we are motivated to examine the relationship between these long-lived CEs and multiple CE formation occurrences and triple eyewall formation. Yang et al. (2013), Yang et al., 2014a, 2014b identified multiple CE formations where CE formed more than once in a TC life cycle, such as Typhoon Winnie (1997) shown in Figure 4. Among the long-lived cases examined in this study, Typhoon Winnie (1997) is the largest typhoon in the WNP with large eyewalls for a long duration. Typhoon Winnie had two CE periods with duration times of 20 and 46.5 h, respectively. The rain rate and SSMI 85 GHz brightness temperature image of Winnie's second CE period are shown in Figure 4. The inner eyewall radius, moat width, and outer eyewall width of Typhoon Winnie, as determined from the satellite images, were 17 (55) km, 57 (137) km, and 40 (137) km in the first (second) CE period. Note that both the rain rate (Figure 4b) and the T_B (Figure 4a) of Winnie are concentric and quite symmetric in the outer eyewall ring. The large size of the moat and the outer eyewall width are essential characteristics of the long-lived CE cases (Figure 1) as well as the multiple CE formation TCs (Yang et al., 2013; Yang et al., 2014a, 2014b).

As an example of the triple eyewalls, Figure 5 shows the triple eyewalls observed in Typhoon Bolaven (2012). The duration of the triple eyewall in Bolaven was 26 h. Multiple microwave satellites observed triple low-brightness-temperature rings (Figures 5a, 5c and 5e). The triple-eyewall TCs often exhibit over open oceans with few surface observations. In the case of Bolaven, surface weather radars high-frequently observed triple heavy precipitation rings every 10 min (Figures 5b, 5d and 5f), in general agreement with the microwave images. Quantitative estimation of the microwave T_B based on our objective methodology

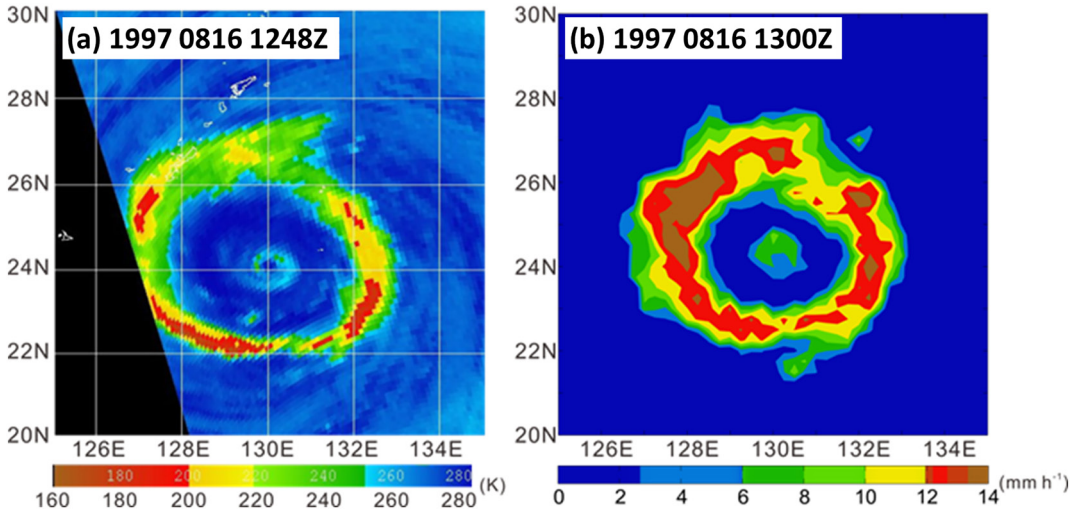

Figure 4. The left panel shows the 85-GHz brightness temperature of Typhoon Winnie (1997) at 1248 UTC on August 16, 1997. The right panel is drawn according to the precipitation rate derived from SSMI satellite observations.

clarified that the tertiary eyewall in Bolaven had a clear concentric structure (Figure 5g). Tsujino et al. (2017) suggested that maintenance of the CEs structure can be induced by the insufficient cutoff of boundary layer inflow in the outer eyewall based on the numerical simulation. Figure 6 gives two examples of triple eyewalls changed to the CE structure. It is clear from Figure 6 that the moat size increased from the change of triple eyewalls to the CE structure. In general agreement with the large size moat, both CE cases are in the long-lived CE category.

The contribution of various CE types (i.e., the formation order of multiple CE formation or triple eyewall) to CE duration is examined (Figure 7). The stacked bar's color represents the order in which the CE is formed during the entire TC lifetime. Whereas Figure 7a presents the numbers, Figure 7b presents the percentages with respect to the case number of each bar. Generally, Figure 7 shows that, as the CE duration longer, the proportion of CEs with a formation order larger than two higher. It is implied that a TC that can exhibit multiple CE formation may also have the conditions to maintain a long-lived CE. Moreover, it is worth noting that there were 7 TC cases of triple eyewalls identified in this study with the techniques modified from Yang et al. (2013). We found that, except for the two cases close to the land, the remaining five triple eyewalls belong to the long-lived CE category.

3.3. Influence of Environmental Factors on CE Durations

The composites of SST, 850–200-mb VWS, 850–700-mb relative humidity (RH), 850-mb divergence and ocean heat content (OHC) are constructed with respect to the CE formation time using SHIPS and STIPS data (Figure 8). On average, the SST (Figure 8a) has decreasing trends in all basins, and the trend is slower in the ATL basin than in the WNP basin. Besides, the SST of long-lived CE cases decreases slower than that in short-lived CE cases in the WPAC and ATL basins (note that EPAC only has two long-lived CE cases). It is suggested that the maintained SST is favorable for maintaining the TC outer eyewall, thereby extending the CE duration.

Another novel finding here is that the VWS is about the same before the CE formation but increases for short-lived CEs and decreases for the long-lived ones (Figure 8b). As the VWS is a well-known factor that is destructive to axisymmetric TC convective features, the increased VWS for a short-lived case is expected to weaken either the inner or outer eyewall and lead to the termination of the CE.

RH for long-lived and short-lived CE cases are also examined (Figure 8c). It is noticed that the RH has significant gaps among basins, with the EPAC having the highest magnitude followed by WNP, and the ATL has the smallest. However, RH is not a factor in determining the CE duration. The RH differences are only 5% in 850–700-mb between long-lived and short-lived CE cases for the three basins.

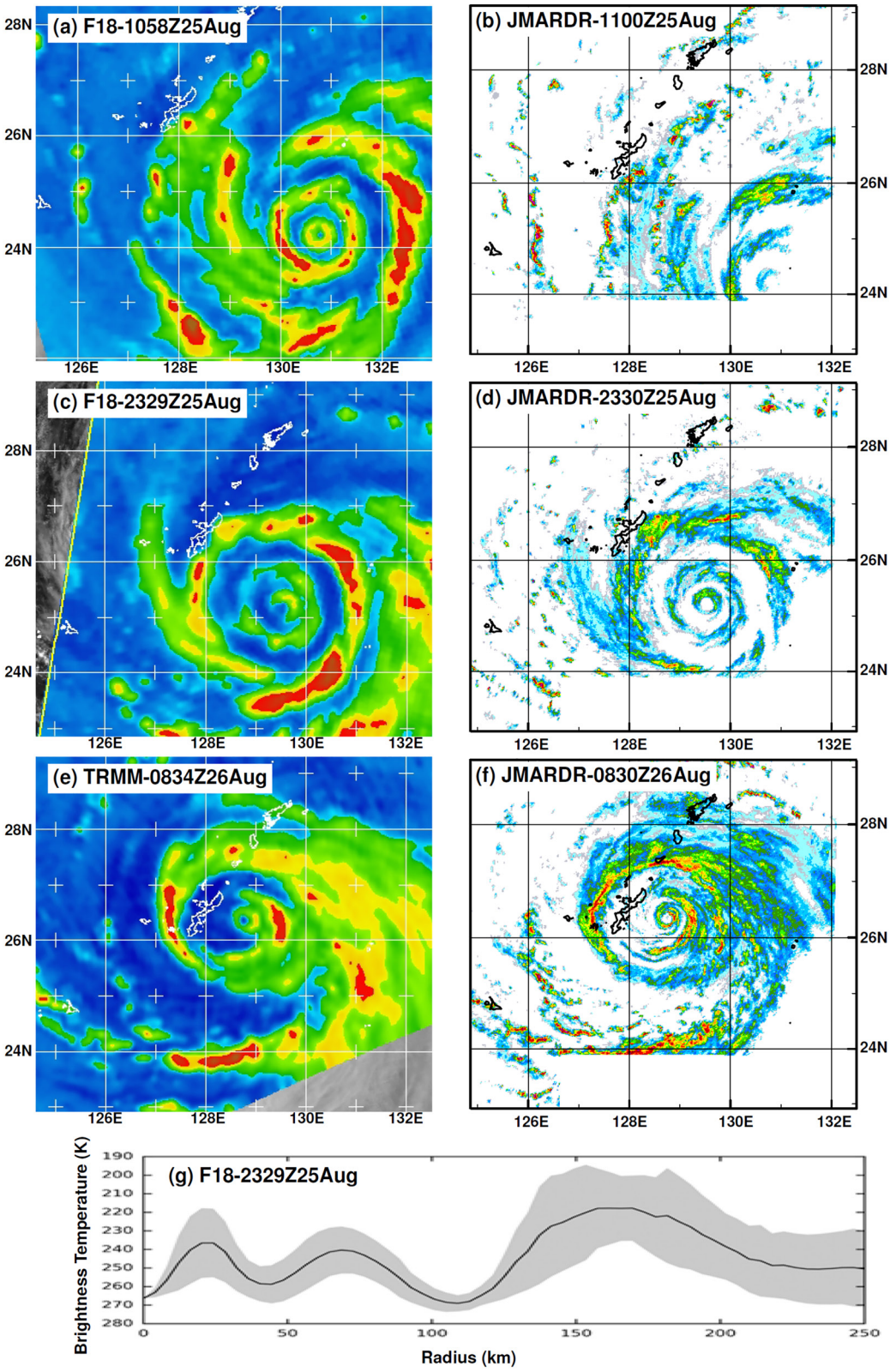

Figure 5. Microwave images from the SSMI/S and TMI at (a) 1058 UTC 25, (c) 2329 UTC 25 and (e) 0834 UTC August 26, 2012; and radar images from Japanese Meteorological Agency (JMA) radar at (b) 1100 UTC 25, (d) 2330 UTC 25 and (f) 0830 UTC August 26, 2012. (g) The Cross-section of inverted brightness temperature from (c) of Typhoon Bolaven (2012).

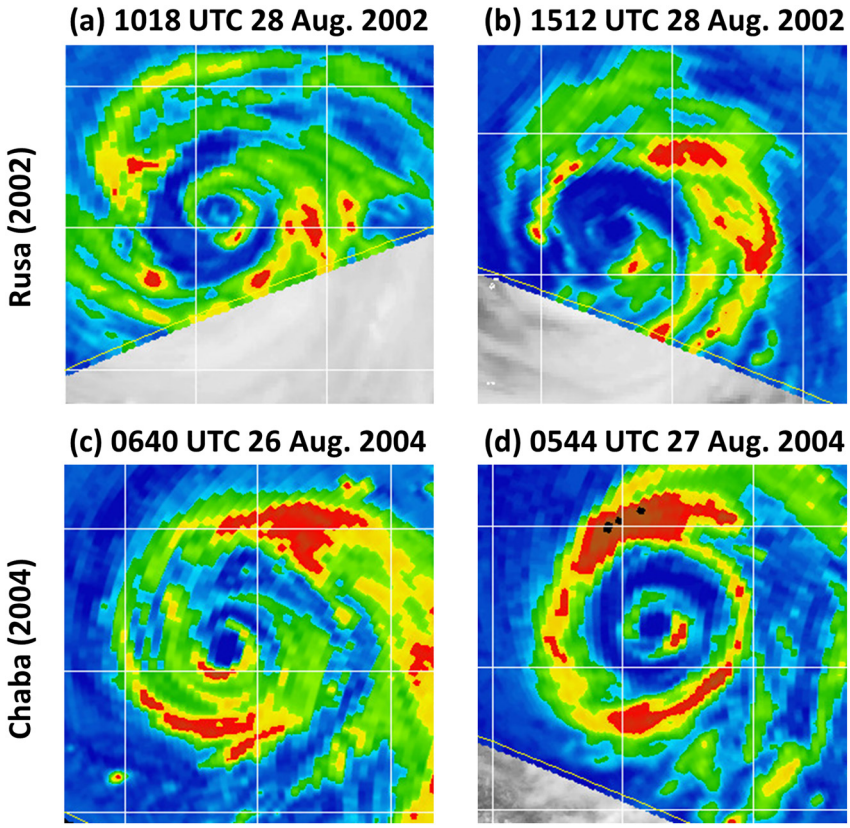

Figure 6. Examples of triple eyewalls observed by microwave satellites. The triple eyewalls in Typhoons (a) Rusa (2002) and (c) Chaba (2004) transformed into CE structures in panels (b) and (d), respectively.

Except for the long-lived CEs in the WNP, Figure 8d shows an increase in intensity before the CE formation time and a decrease afterward, while the trend is subtle but still there for WNP CEs with durations <20 h. The intensity trend is consistent with the detailed aircraft and other observations in the Atlantic upon which the modern understanding is based (Sitkowski et al., 2011). Note again that the discrepancy regarding long-lived CEs in the WNP is possibly due to the failure of the Dvorak technique capturing intensity fluctuations during the ERCs.

Warm SST is favorable for TC development, and SST is a critical factor in some statistical intensity forecast techniques (DeMaria & Kaplan, 1994). However, SST has shown not to be critical in forecasting rapid intensification and decay (Law & Hobgood, 2007; Schade & Emmanuel, 1999). A quantified measure of the amount of warm, deep water is a better way to measure the amount of energy available to the storm. The oceanic heat content (OHC) is such a variable to measure the heat and amount of warm water available for TCs (Shay & Brewster, 2010; Wada & Usui, 2007). While the SST distribution may be more uniform within a limited range (Figure 8a), considerable OHC variation among basins is observed. In Figure 8e, the WNP has the highest OHC, followed by the ATL, and the EPAC has the lowest. However, the OHC is not a factor to determine the CE duration, presumably because while the OHC is strongly tied to the development of eyewall convection, it is not as sensitive to the development of outer eyewall as the SST is.

To further investigate the SST and VWS factors that may influence the CE duration, TC tracks (Figure 9) and moving directions (Figure 10) are examined. Figure 9 shows the 48-h TC tracks centered at the CE formation time; the blue represents short-lived CE cases (<20 h) while the red represents long-lived CE cases (≥20 h). In both the WNP (Figure 9a) and ATL (Figure 9b) basins, the TC tracks with long-lived CEs tend to locate south of 25°N and west of the basins. It is in general agreement that TCs are more intense after a long journey over the ocean. Also, the long-lived CEs are with a lower northward translation speed. There is almost no long-lived CE track that moves northeast into the mid-latitude westerlies region with large and

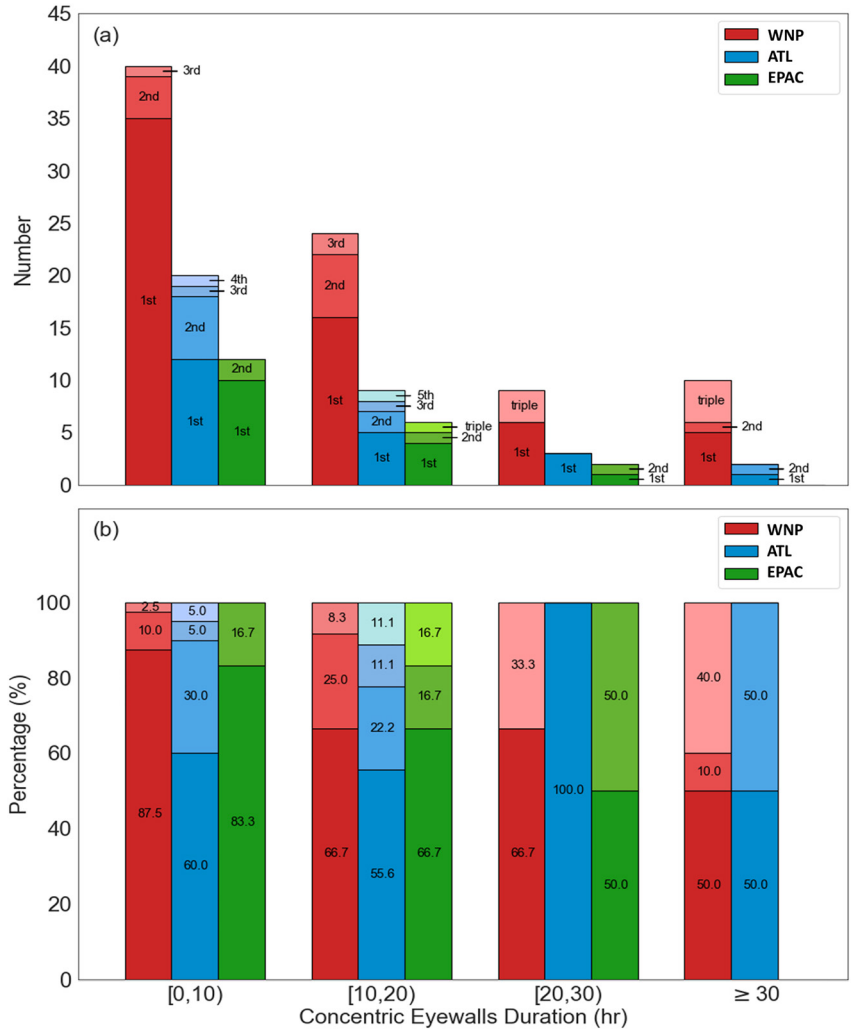

Figure 7. (a) concentric eyewall (CE) case numbers in different basins for various durations. The red, blue, and green bars represent the western North Pacific (WNP), Atlantic (ATL), and eastern Pacific (EPAC) basins, respectively. Shading colors of stacked bars indicate different types of CE [i.e., formation orders in the tropical cyclones (TC) lifetime, or a triple eyewall case; texts in (a)]. (b) As in (a), but the percentages of each bar.

detrimental VWS. By contrast, TC tracks with short-lived CEs tend to have relatively large northward components. The northward motion explains the decreased SST trend and the increased VWS trend (Figures 8a and 8b). The higher SST and weaker VWS seem to be beneficial to the maintenance of the CE structure and the TC's overall intensity. Finally, due to the small sample number of CE in the ENP, no significant difference in TC tracks can be distinguished in Figure 9c.

To further examine whether the long-lived and short-lived CEs have a significant difference in the northward motion, the density distributions of their moving direction are calculated (Figure 10). The calculation is based on tracks in Figure 9, which is −24–24 h with respect to the CE formation time. The result shows that a significant difference can be found in the mean moving directions between different CE durations (Figure 10, dashed lines), based on the Wilcoxon–Mann–Whitney test at the 95% confidence level. Wilcoxon–Mann–Whitney test is a nonparametric test suitable for samples that are not normal; it tests the null hypothesis that, for randomly selected values X and Y from two populations, the probability of X being greater than Y is equal to the probability of Y being greater than X (Fay & Proschan, 2010; Mann & Whitney, 1947). It is suggested that, again, the TC movement distribution associated with long-lived CEs is more concentrated toward the general west direction. On the other hand, the distribution for the short-lived CE group is with a wider distribution of moving direction and a significant mean northward component of motion.

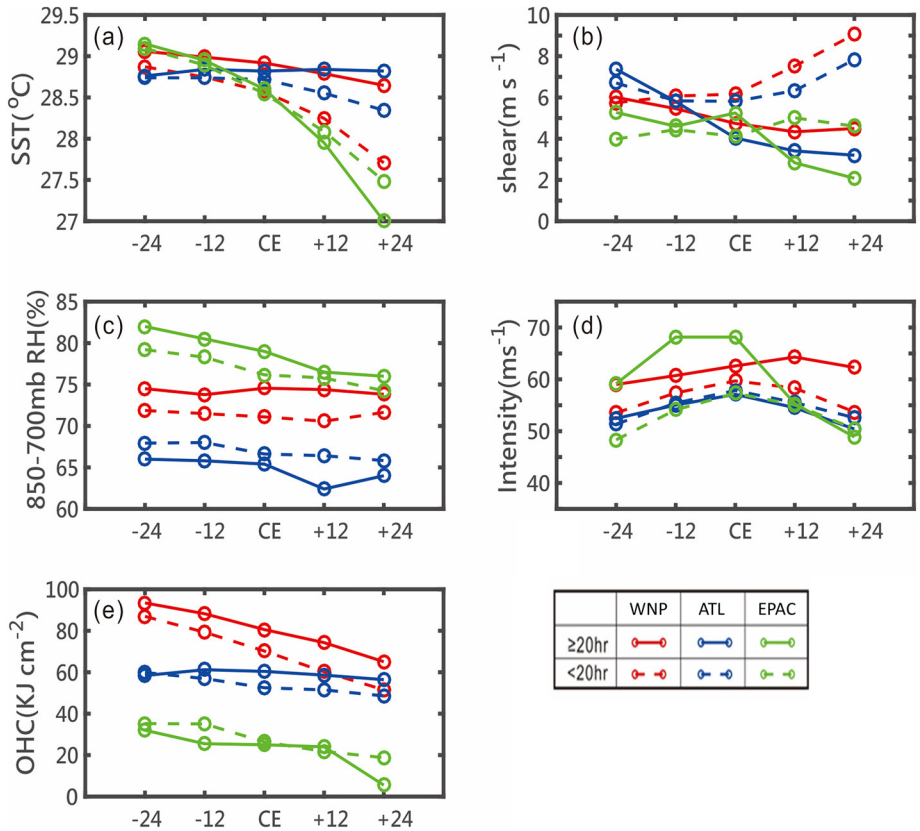

Figure 8. The time series of (a) mean SST, (b) mean 850-200-mb VWS, (c) mean 850-700-mb RH, (d) mean TC intensity, and (e) mean OHC for CE cases in the western North Pacific (WNP) (red), Atlantic (ATL) (blue), and eastern Pacific (EPAC) (green) basins. The solid and dash lines represent the CE cases with a duration longer than and equal to 20 h, and duration less than 20 h. The composites were done relative to the time of concentric eyewall (CE) formation.

In addition to the internal factors (e.g., CE structure and size) related to short-lived CE cases, northward movement may also contribute to the probability of encountering large environmental VWS and cool SST that are detrimental to the CE duration.

Regarding the TC translation speed (Figure 11), long-lived CE cases have significantly slower motion than that of short-lived CE cases, passing Wilcoxon–Mann–Whitney tests at the 95% confidence level. Translation speed larger than 15 km h^{-1} seems detrimental for CE maintenance because TCs with faster speeds tend to be in higher shear conditions and have less time over favorable conditions. In the ATL basin (Figure 11b), long-lived CE cases have a mean translation speed of only 6.8 km $h^{-1,}$ while short-lived cases have a mean translation speed of 10.2 km h^{-1}, suggesting that long-lived cases tend to stay in the same environment during the CE life cycle.

In summary, environmental parameters examined here that deem favorable for the CE formation are also those identified by Kaplan and DeMaria (2003) that are favorable for intensification and are favorable for TC development. Therefore, we link the CEs with the TC intensity, and the results indicate that the environmental factors favorable for TC development are also favorable for long-lived CE duration. The most significant environmental factor separating the short-lived CEs from the long-lived ones is the VWS. The long-lived CE track cannot move north into the mid-latitude westerlies region with large detrimental VWS. Furthermore, a slower translation speed may prolong the CE duration by keeping the TC in a slowly changing environment suitable for CE maintenance.

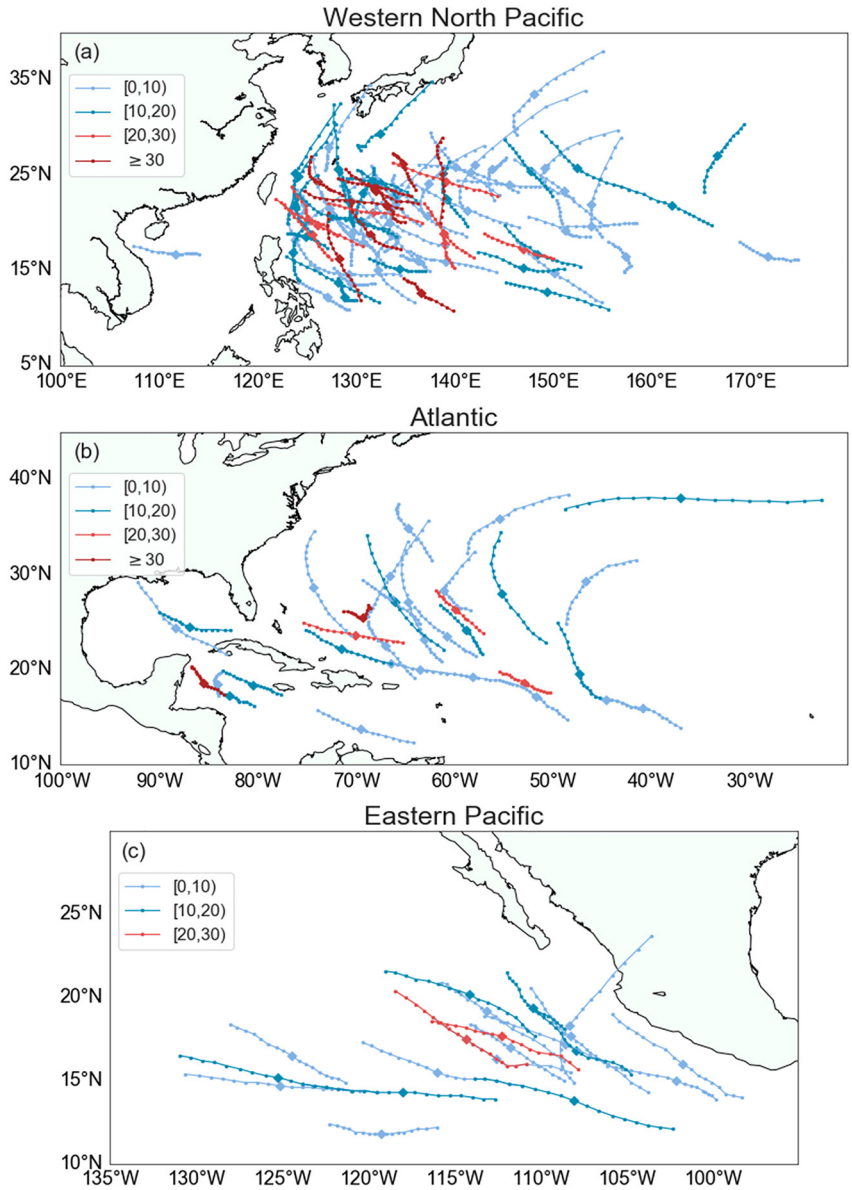

Figure 9. TC tracks in the 48 h centered at the CE formation time in (a) western North Pacific (WNP), (b) Atlantic (ATL), and (c) eastern Pacific (EPAC). The red colors and blue colors represent long-lived and short-lived CE cases. The diamond indicates the location of concentric eyewall (CE) formation, and the dots indicate TC locations every three h.

4. Summary

This study investigates the climatological characteristics of the long-lived CEs and triple eyewalls within TCs. The primary data used are satellite images from SSM/I and TMI, covering 1997 to 2014. Composites of environmental parameters from SHIPS and STIPS are constructed to reveal the environment's impacts on the formation of CEs and their durations.

The structural characteristics of a CE are defined by its inner core size, the moat size, and the outer eyewall width. CEs are grouped into four categories with various durations: less than 10 h, between 10 and 20 h, between 20 and 30 h, and those greater than 30 h. This study examined 83, 34, and 26 CE cases in the WNP, ATL, and EPAC basins. A long-lived case generally has a large moat and outer eyewall. The outer eyewall width and moat width are well correlated in the WNP and ATL basins. Larger outer eyewall contains more cloud liquid water, maybe with more massive latent heat release. Furthermore, the outer eyewall width is

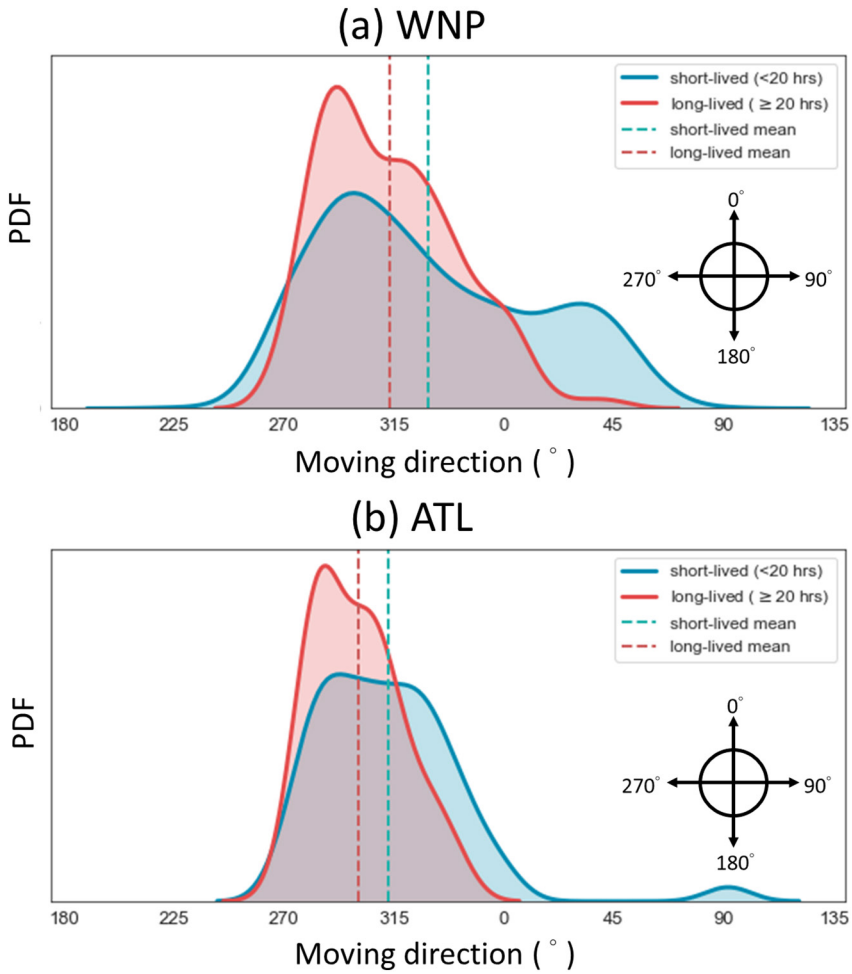

Figure 10. The probability distributions (*Y*-axis) of tropical cyclones (TC) moving direction for the long-lived (red) and short-lived (blue) CE cases in (a) western North Pacific (WNP) and (b) Atlantic (ATL). The moving direction of 270° indicates westward motion, while 0° indicates northward motion.

about the same in WNP and ATL, and they increase with the increase of the CE duration. Within the three structural parameters, the inner eyewall size is larger in the ATL, and the moat and the outer eyewall width are larger in the WNP. This study also identified seven triple-eyewall typhoons in the WNP, with five of them belongs to the long-lived CE category. In some of the triple eyewall cases, it changed to a CE structure with an extensive moat size. The large moat size may delay the ERC and affect the TC intensity change.

Another novel result of this study is that, in addition to the internal dynamical processes, favorable environmental conditions are also crucial to the prolonged CE duration. Several environmental factors, including SST, VWS, RH, and OHC, are examined for long-lived and short-lived CEs, and the result suggests that higher SST and lower VWS are critical to control the CE duration. The most considerable environmental difference distinguishing the short- and long-lived CEs is the VWS. The short-lived CEs suffer a large increase of the VWS after the formation while the long-lived ones have their environmental shear decreases. Furthermore, our analysis suggests that TCs with a long-lived CE tend to have less northward motion and reside in a TC-favorable environmental condition for a longer time. The long-lived CE mainly occurred south of 25°N in both WNP and ATL basins.

Based on the records of 83 CE cases in the WNP during 1997–2014, as identified by Yang et al. (2013), the correlations of intensity estimates for these CE storms between the Japanese Meteorological Agency (JMA) and Joint Typhoon Warning Center (JTWC) were calculated (not shown). It is noted that at 12 h before the CE formation time, the intensity correlation of both agencies decreases from 90% to 60% and remains

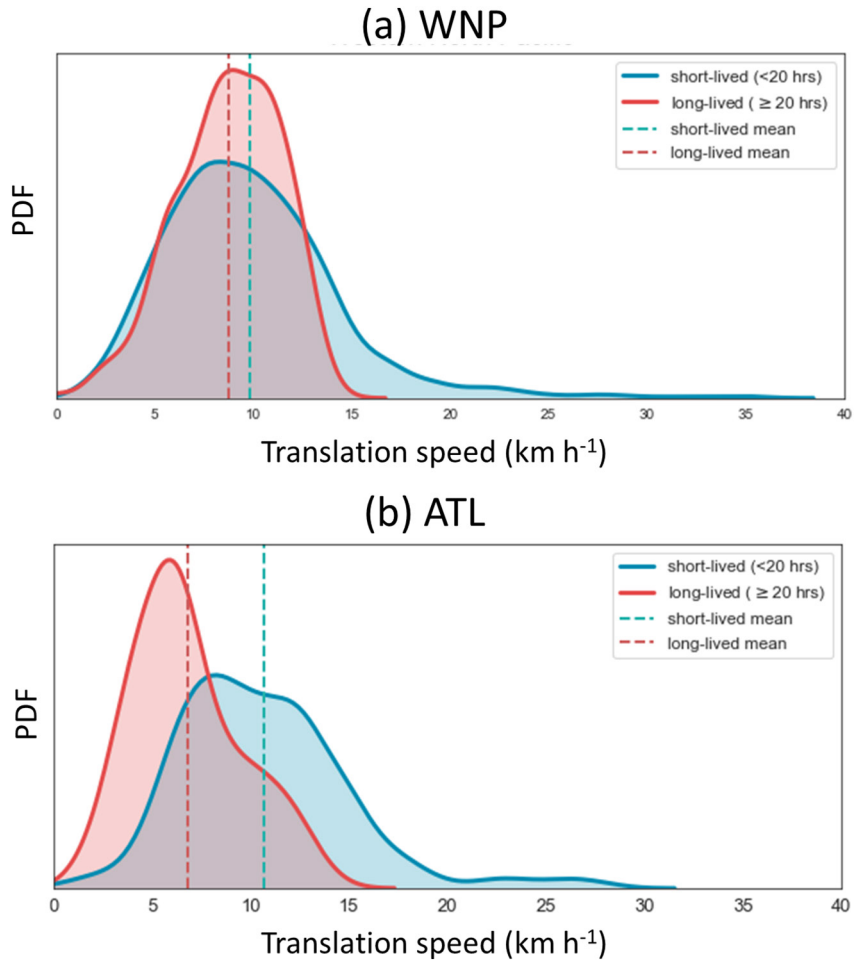

Figure 11. The probability distributions (*Y*-axis) of tropical cyclones (TC) translation speed for the long-lived (red) and short-lived (blue) concentric eyewall (CE) cases in (a) western North Pacific (WNP) and (b) Atlantic (ATL).

low for the following 60 h. The calculation suggests that the ERC process and CE duration also have a considerable impact on operational TC intensity estimation by the Dvorak technique. Our paper suggests future modification of the conceptual model and forecast guidance for the CE forecasting to including the potential impacts from the external environmental factors and internal structure factors. Moreover, when interpreting high-resolution numerical forecasts of ERC development, the forecaster should pay attention to the vortex structure and the trends and variability of the environmental VWS and TC tracks to help determine the possible CE duration.

Yang et al. (2015) suggested that cases of multiple CE formation with large size are more likely to occur in warm and normal ENSO episodes. Our result, consistent with Yang et al. (2015), shows that long-lived CE duration may be resulted from the multiple CE formation. It is also possible that, during an El Nino year, WNP TCs with long-lived CEs tend to have less northward motion due to the east-west extended sub-tropical high and stay away from the environment with detrimental SST and VWS. In summary, it is implied that the CE internal dynamical process, the CE tracks, and the environmental conditions are all essential for the CE size and duration. From a climatological perspective, future works can investigate the contribution to the accumulated cyclone energy or integrated kinetic energy for TCs with CEs during different ENSO episodes and further evaluate the impact of CEs in numerical ensemble models for sub-seasonal to seasonal forecasts.

Data Availability Statement

The microwave images utilized in this study were provided by the Tropical Cyclone Pages in the Naval Research Laboratory (https://www.nrlmry.navy.mil/TC.html). The JMA radar data in Figure 5 were provided by the Global Atmospheric Observation Data project in Kyoto University (http://database.rish.kyoto-u.ac.jp/arch/jmadata/data/jma-radar/synthetic/original/).

Acknowledgments
This work was supported by MOST Taiwan (Ministry Of Science and Technology in Taiwan) under grant MOST-106-2119-M-002-016, MOST 109-2111-M-002-008, MOST 109-2625-M-002-021, and the Office of Naval Research Global under grant N62909-15-1-2008. The authors thank Ms. Chun-Min Hsiao of NTU for her efforts in preparing several figures in this manuscript.

References

Abarca, S. F., & Corbosiero, K. L. (2011). Secondary eyewall formation in WRF simulations of Hurricanes Rita and Katrina (2005). *Geophysical Research Letters*, *38*. L07802. https://doi.org/10.1029/2011gl047015

Black, M. L., & Willoughby, H. E. (1992). The concentric eyewall cycle of Hurricane Gilbert. *Monthly Weather Review*, *120*, 947–957. https://doi.org/10.1175/1520-0493(1992)120<0947:tcecoh>2.0.co;2

DeMaria, M., & Kaplan, J. (1994). A statistical hurricane intensity prediction scheme (SHIPS) for the Atlantic basin. *Weather and Forecasting*, *9*, 209–220. https://doi.org/10.1175/1520-0434(1994)009<0209:aships>2.0.co;2

DeMaria, M., & Kaplan, J. (1999). An updated statistical hurricane intensity prediction scheme (SHIPS) for the Atlantic and eastern North Pacific basins. *Weather and Forecasting*, *14*, 326–337. https://doi.org/10.1175/1520-0434(1999)014<0326:auship>2.0.co;2

DeMaria, M., Mainelli, M., Shay, L. K., Knaff, J. A., & Kaplan, J. (2005). Further improvement to the Statistical Hurricane Intensity Prediction Scheme (SHIPS). *Weather and Forecasting*, *20*, 531–543. https://doi.org/10.1175/waf862.1

Fay, M. P., & Proschan, M. A. (2010). Wilcoxon–Mann–Whitney or t-test? On assumptions for hypothesis tests and multiple interpretations of decision rules. *Statistics Surveys*, *4*, 1–39. MR 2595125. PMC 2857732. PMID 20414472. https://doi.org/10.1214/09-SS051

Greenwald, T. J., Stephens, G. L., Christopher, S. A., & Vonder Haar, T. H. (1995). Observations of the global characteristics and regional radiative effects of marine cloud liquid water. *Journal of Climate*, *8*, 2928–2946. https://doi.org/10.1175/1520-0442(1995)008<2928:ootgca>2.0.co;2

Hawkins, J. D., & Helveston, M. (2004). Tropical cyclone multiple eyewall characteristics. In *Preprints, 26th conf. On Hurricane and tropical Meteorology* (pp. 276–277). Amer. Meteor. Soc. Retrieved from https://ams.confex.com/ams/26HURR/techprogram/paper_76084.htm

Hawkins, J. D., & Helveston, M. (2008). Tropical cyclone multiple eyewall characteristics. In *28th conference on hurricanes and tropical Meteorology*. Amer. Meteor. Soc. 6B.1. Retrieved from http://ams.confex.com/ams/28Hurricanes/techprogram/paper_138300.htm

Hawkins, J. D., Helveston, M., Lee, T. F., Turk, F. J., Richardson, K., Sampson, C., et al. (2006). Tropical cyclone multiple eyewall characteristics. In *Preprints, 27th conf. On Hurricane and tropical Meteorology*. Amer. Meteor. Soc. 6B.1. Retrieved from http://ams.confex.com/ams/27Hurricanes/techprogram/paper_108864.htm

Hawkins, J. D., Lee, T. F., Turk, F. J., Sampson, C., Kent, J., & Richardson, K. (2001). Real-time Internet distribution of satellite products for tropical cyclone reconnaissance. *Bulletin of the American Meteorological Society*, *82*, 567–578. https://doi.org/10.1175/1520-0477(2001)082<0567:ridosp>2.3.co;2

Hawkins, J. D., Turk, F. J., Lee, T. F., & Richardson, K. (2008). Observations of tropical cyclones with the SSMIS. *IEEE Transactions on Geoscience and Remote Sensing*, *46*, 901–912. https://doi.org/10.1109/tgrs.2008.915753

Kaplan, J., & DeMaria, M. (2003). Large-scale characteristics of rapidly intensifying tropical cyclones in the North Atlantic basin. *Weather and Forecasting*, *18*, 1093–1108. https://doi.org/10.1175/1520-34(2003)018<1093:LCORIT>2.0.CO;

Knaff, J. A., Sampson, C. R., & DeMaria, M. (2005). An operational statistical typhoon intensity prediction scheme for the Western North Pacific. *Weather Forecasting*, *20*, 688–699. https://doi.org/10.1175/waf863.1

Kossin, J. P., Schubert, W. H., & Montgomery, M. T. (2000). Unstable interaction between a hurricane's primary eyewall and a secondary ring of enhanced vorticity. *Journal of the Atmospheric Sciences*, *57*, 3893–3917. https://doi.org/10.1175/1520-0469(2001)058<3893:uibahs>2.0.co;2

Kummerow, C., Barnes, W., Kozu, T., Shiue, J., & Simpson, J. (1998). The Tropical Rainfall Measuring Mission (TRMM) sensor package. *Journal of Atmospheric and Oceanic Technology*, *15*, 809–817. https://doi.org/10.1175/1520-0426(1998)015<0809:ttrmmt>2.0.co;2

Kuo, H.-C., Chang, C.-P., Yang, Y.-T., & Jiang, H.-J. (2009). Western North Pacific typhoons with concentric eyewalls. *Monthly Weather Review*, *137*, 3758–3770. https://doi.org/10.1175/2009mwr2850.1

Kuo, H.-C., Lin, L.-Y., Chang, C.-P., & Williams, R. T. (2004). The formation of concentric vorticity structures in typhoons. *Journal of the Atmospheric Sciences*, *61*, 2722–2734. https://doi.org/10.1175/jas3286.1

Law, K. T., & Hobgood, J. S. (2007). A statistical model to forecast short-term atlantic hurricane intensity. *Weather and Forecasting*, *22*, 967–980. https://doi.org/10.1175/waf1027.1

Lin, B., & Rossow, W. B. (1994). Observations of cloud liquid water path over oceans: Optical and microwave remote sensing methods. *Journal of Geophysical Research*, *99*, 20907–20927. https://doi.org/10.1029/94JD01831

Liu, G., & Curry, J. A. (1993). Determination of characteristics of cloud liquid water from satellite microwave measurements. *Journal of Geophysical Research*, *98*, 5069–5092. https://doi.org/10.1029/92jd02888

Maclay, K. S., DeMaria, M., & Vonder Haar, T. H. (2008). Tropical cyclone inner core kinetic energy evolution. *Monthly Weather Review*, *136*, 4882–4898. https://doi.org/10.1175/2008mwr2268.1

Mann, H. B., & Whitney, D. R. (1947). On a test of whether one of two random variables is stochastically larger than the other. *Annals of Mathematical Statistics*, *18*(1), 50–60. MR 0022058. Zbl 0041.26103. https://doi.org/10.1214/aoms/1177730491

McNoldy, B. D. (2004). Triple eyewall in Hurricane Juliette. *Bulletin of the American Meteorological Society*, *85*, 1663–1666. https://doi.org/10.1175/bams-85-11-1663

Montgomery, M. T., Zhang, J. A., & Smith, R. K. (2014). An analysis of the observed low-level structure of rapidly intensifying and mature hurricane Earl (2010). *Quarterly Journal of the Royal Meteorological Society*, *140*(684), 2132–2146. https://doi.org/10.1002/qj.2283

Ortt, D., & Chen, S. S. (2008). Effect of environmental moisture on rainbands in Hurricane Rita and Katrina (2005). *28th Conference on Hurricane and Tropical Meteorology, American Meteorological Society, Miami, FL, Amer. Meteor. Soc.* preprint 5C.5.

Petty, G. W. (1990). *On the response of the Special Sensor Microwave/Imager on the marine environment Implications for atmospheric parameter retrievals* (p. 291). Univ. of WA.

Qiu, X., Tan, Z.-M., & Xiao, Q. (2010). The roles of vortex Rossby waves in hurricane secondary eyewall formation. *Monthly Weather Review*, *138*, 209–2109. https://doi.org/10.1175/2010mwr3161.1

Rozoff, C. M., Nolan, D. S., Kossin, J. P., Zhang, F. Q., & Fang, J. (2012). The roles of an expanding wind field and inertial stability in tropical cyclone secondary eyewall formation. *Journal of the Atmospheric Sciences*, *69*, 2621–2643. https://doi.org/10.1175/jas-d-11-0326.1

Schade, L. K., & Emmanuel, K. A. (1999). The ocean's effect on the intensity of tropical cyclones: Results from a simple coupled atmosphere-ocean model. *Journal of the Atmospheric Sciences*, *56*, 642–651. https://doi.org/10.1175/1520-0469(1999)056<0642:toseot>2.0.co;2

Shay, L. K., & Brewster, J. K. (2010). Oceanic heat content variability in the Eastern Pacific Ocean for hurricane intensity forecasting. *Monthly Weather Review*, *138*, 2110–2131. https://doi.org/10.1175/2010mwr3189.1

Sitkowski, M., Kossin, J. P., & Rozoff, C. M. (2011). Intensity and structure changes during hurricane eyewall replacement cycles. *Monthly Weather Review*, *139*, 3829–3847. https://doi.org/10.1175/mwr-d-11-00034.1

Terwey, W. D., & Montgomery, M. T. (2008). Secondary eyewall formation in two idealized, full-physics modeled hurricanes. *Journal of Geophysical Research*, *113*. D12112. https://doi.org/10.1029/2007JD008897

Tsujino, S., Tsuboki, K., & Kuo, H. (2017). Structure and maintenance mechanism of long-lived concentric eyewalls associated with simulated Typhoon Bolaven (2012). *Journal of the Atmospheric Sciences*, *74*, 3609–3634. https://doi.org/10.1175/JAS-D-16-0236.1

Wada, A., & Usui, N. (2007). Importance of tropical cyclone heat potential for tropical cyclone intensification in the Western North Pacific. *Journal of Oceanography*, *63*(3), 427–447. https://doi.org/10.1007/s10872-007-0039-0

Wentz, F. J. (2013). *SSM/I Version-7 calibration report, report number 011012* (p. 46pp). Remote Sensing Systems

Wentz, F. J., & Meissner, T. (2000). *AMSR ocean algorithm (Version 2) algorithm theoretical basis document (ATBD), RSS technical report 121599A-1*. Remote Sensing Systems. Retrieved from http://www.remss.com/papers/amsr/AMSR_Ocean_Algorithm_Version_2.pdf

Willoughby, H. E. (1995). Mature structure and evolution. In *Chapter 2, global perspectives on tropical cyclones (WMO/TD-No. 693, report No. TCP-38)*. World Meteorological Organization.

Willoughby, H. E., & Black, P. G. (1996). Hurricane Andrew in Florida: Dynamics of a disaster. *Bulletin of the American Meteorological Society*, *77*, 543–549. https://doi.org/10.1175/1520-0477(1996)077<0543:haifdo>2.0.co;2

Willoughby, H. E., Clos, J. A., & Shoreibah, M. G. (1982). Concentric eye walls, secondary wind maxima, and the evolution of the hurricane vortex. *Journal of the Atmospheric Sciences*, *39*, 395–411. https://doi.org/10.1175/1520-0469(1982)039<0395:cewswm>2.0.co;2

Yang, S., Bankert, R., & Cossuth, J. (2020). Tropical cyclone climatology from satellite passive microwave measurements. *Remote Sensing*, *12*(21), 3610. https://doi.org/10.3390/rs12213610

Yang, S., & Cossuth, J. (2016). Satellite remote sensing of tropical cyclones. In *Chapter 7, recent developments in tropical cyclone dynamics, prediction, and detection* (pp. 138–170). INTECH. https://doi.org/10.5772/64114

Yang, S., Hawkins, J., & Richardson, K. (2014a). The improved NRL tropical cyclone monitoring system with a unified microwave brightness temperature calibration scheme. *Remote Sensing*, *6*, 4563–4581. https://doi.org/10.3390/rs6054563

Yang, Y.-T., Hendricks, E. A., Kuo, H.-C., & Peng, M. S. (2014b). Long-lived concentric eyewalls in Typhoon Soulik (2013). *Monthly Weather Review*, *142*, 3365–3371. https://doi.org/10.1175/mwr-d-14-00085.1

Yang, Y.-T., Kuo, H.-C., Hendricks, E., & Peng, M. S. (2013). Structural and intensity changes of concentric eyewall typhoons in the Western North Pacific Basin. *Monthly Weather Review*, *141*(8), 2632–2648. https://doi.org/10.1175/mwr-d-12-00251.1

Yang, Y.-T., Kuo, H.-C., Hendricks, E., & Peng, M. S. (2016). Satellite climatology of tropical cyclone with concentric eyewalls. In *Chapter 8. Recent developments in tropical cyclone dynamics, prediction, and detection* (pp. 171–190). InTech (ISBN:978-953-51-2703-1).

Yang, Y.-T., Kuo, H.-C., Hendricks, E. A., Liu, Y., & Peng, M. S. (2015). Relationship between typhoons with concentric eyewalls and ENSO in the western North Pacific basin. *Journal of Climate*, *28*, 3612–3623. https://doi.org/10.1175/JCLI-D-14-00541.1

Zhao, K., Lin, Q., Lee, W.-C., Sun, Y. Q., & Zhang, F. (2016). Dopplar radar analysis of triple eyewalls in typhoon Usagi (2013). *Bulletin of the American Meteorological Society*, *97*, 25–30. https://doi.org/10.1175/bams-d-15-00029.1

Zhou, X., & Wang, B. (2009). From concentric eyewall to annular hurricane: A numerical study with the cloud-resolved WRF model. *Geophysical Research Letters*, *36*. L03802. https://doi.org/10.1029/2008GL036854